

Accepted Manuscript

Anomalous local lattice disorder and distortion in $A_2\text{Mo}_2\text{O}_7$ pyrochlores

C. Castellano, G. Berti, F. Rubio-Marcos, G. Lamura, S. Sanna, E. Salas-Colera, A. Brambilla, Á. Muñoz-Noval, L. Duò, F. Demartin



PII: S0925-8388(17)32280-6

DOI: [10.1016/j.jallcom.2017.06.272](https://doi.org/10.1016/j.jallcom.2017.06.272)

Reference: JALCOM 42341

To appear in: *Journal of Alloys and Compounds*

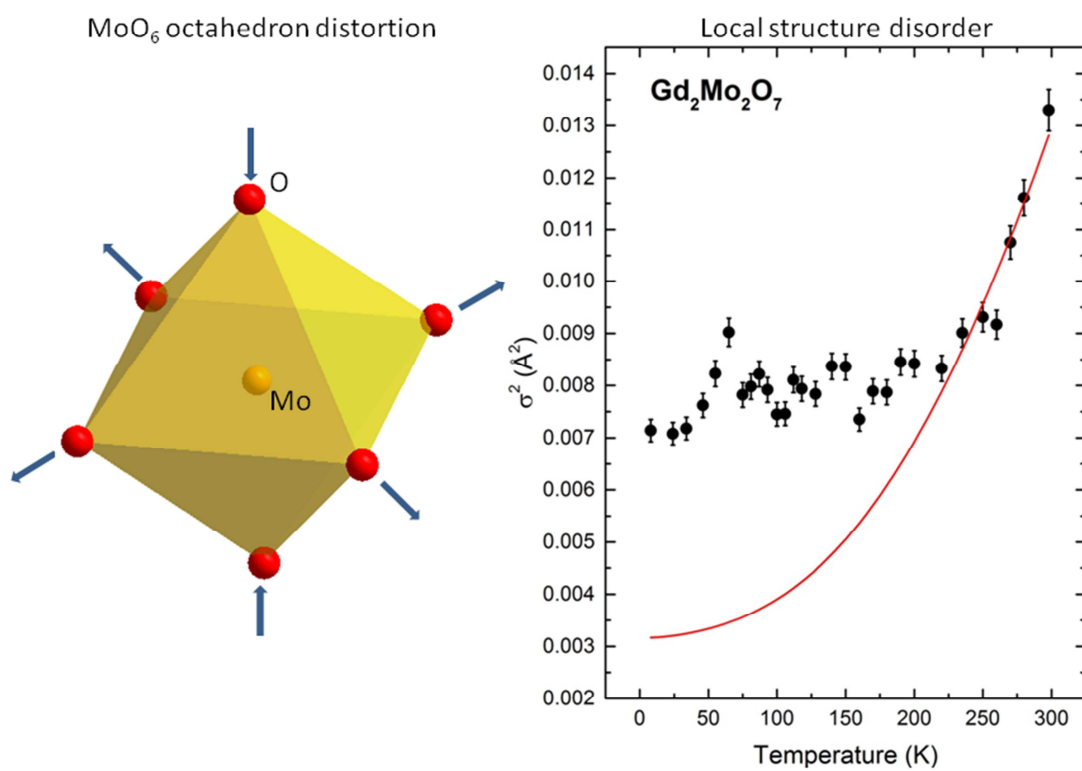
Received Date: 12 April 2017

Revised Date: 12 June 2017

Accepted Date: 24 June 2017

Please cite this article as: C. Castellano, G. Berti, F. Rubio-Marcos, G. Lamura, S. Sanna, E. Salas-Colera, A. Brambilla, Á. Muñoz-Noval, L. Duò, F. Demartin, Anomalous local lattice disorder and distortion in $A_2\text{Mo}_2\text{O}_7$ pyrochlores, *Journal of Alloys and Compounds* (2017), doi: 10.1016/j.jallcom.2017.06.272.

This is a PDF file of an unedited manuscript that has been accepted for publication. As a service to our customers we are providing this early version of the manuscript. The manuscript will undergo copyediting, typesetting, and review of the resulting proof before it is published in its final form. Please note that during the production process errors may be discovered which could affect the content, and all legal disclaimers that apply to the journal pertain.



ACCEPTED

Anomalous local lattice disorder and distortion in $A_2Mo_2O_7$ pyrochlores

C. Castellano^{a,*}, G. Berti^{b,**}, F. Rubio-Marcos^c, G. Lamura^d, S. Sanna^e, E. Salas-Colera^{f,g}, A. Brambilla^b, Á. Muñoz-Noval^h, L. Duò^b, F. Demartin^a

^a Dipartimento di Chimica, Università degli Studi di Milano, via Golgi 19, 20133 Milano, Italy

^b Dipartimento di Fisica, Politecnico di Milano, piazza Leonardo da Vinci 32, 20133 Milano, Italy

^c Electroceramic Department, Instituto de Cerámica y Vidrio, CSIC, Kelsen 5, 28049 Madrid, Spain

^d CNR-SPIN, corso Perrone 24, 16146 Genova, Italy

^e Department of Physics and Astronomy, University of Bologna, 40127 Bologna, Italy

^f Instituto de Ciencia de Materiales de Madrid, ICMM, CSIC, Sor Juana Inés de la Cruz 3, 28049, Cantoblanco, Madrid, Spain

^g Spanish CRG BM25 SpLine, ESRF 71 Avenue des Martyrs CS 40220 FR - 38043 Grenoble, France

^h Department of Applied Chemistry, Hiroshima University, 1-4-1 Kagamiyama, Higashi-Hiroshima, Hiroshima 739-8527, Japan

*Corresponding author. E-mail address: carlo.castellano@unimi.it

**Present address: Department of Chemical Physics, Fritz-Haber-Institut der Max-Planck-Gesellschaft, Faradayweg 4-6, 14195 Berlin, Germany

Abstract

We present an extended X-ray absorption fine structure study of the pyrochlores $A_2Mo_2O_7$ ($A = \text{Gd, Dy, Ho, Er}$), as a function of temperature. While in the three spin-glass compositions $\text{Dy}_2\text{Mo}_2\text{O}_7$, $\text{Ho}_2\text{Mo}_2\text{O}_7$ and $\text{Er}_2\text{Mo}_2\text{O}_7$ the Debye temperatures are in accordance with other pyrochlores and the static disorder contributions are compatible with a lattice frustration, in the low-temperature-ferromagnetic $\text{Gd}_2\text{Mo}_2\text{O}_7$ system we point out an anomalous enhancement of the local structure disorder below about 225 K down to low temperatures. Moreover, considering the general pyrochlore predisposition towards structural disorder, we prove the presence on a local scale of at least a bimodal distribution of the Mo-O(1) octahedral interatomic distances for all the studied compounds, consisting of two shorter and four longer bond lengths. Our results suggest that the local structure order parameter plays an important role in the ferromagnetic or spin-glass phase stabilization.

Keywords: A. Oxide materials; A. Pyrochlores; C. order-disorder effects; D. EXAFS

1. Introduction

Complex pyrochlore oxides with general formula $A_2^{3+}B_2^{4+}O(1)_6(O_2)$, where A is a trivalent rare-earth ion including lanthanides, Y, or Sc and B is usually a tetravalent transition metal or a p-block metal ion, display a wide range of interesting physical properties. Pyrochlores crystallize in the

cubic space group $Fd\bar{3}m$ closely related to the fluorite structure (CaF_2) but with the presence of two cation sites and the absence of 1/8 of the oxygen anions [1]. Both the A and B sites form a network of corner-sharing tetrahedra characteristic of a geometrically frustrated magnet, resulting in some intriguing short-range ordered phases at low temperature, such as spin glasses, spin ices and spin liquids. This kind of network is found in several common minerals as in the octahedrally coordinated B site of the spinel class (AB_2O_4), where B is a trivalent magnetic transition metal ion. Interesting topics with respect to pyrochlores include a large variety of magneto-conductive properties such as metal-insulator transitions, magnetic frustration, magnetoresistance, superconductivity, ferroelectricity, ionic and mixed conductivity, pigments and catalysis and their use as an inert matrix for nuclear fuel and waste immobilization [1,2].

Recently, special attention has been devoted to those pyrochlores where glassy transitions occur upon varying the chemical composition and temperature. In other compounds of the same family a long-range ordered state can also persist. This latter is promoted by spin-spin and neighbor exchange interactions, as in the ferromagnetic (FM) $\text{A}_2\text{Mo}_2\text{O}_7$ ($A = \text{Nd, Sm and Gd}$) and $\text{A}_2\text{Mn}_2\text{O}_7$ (with a small rare earth $A = \text{Sc, Tb-Lu or Y}$) [3-5]. The mean rare earth ionic radius r_A influences the magnetic ground state, i.e. the FM or spin-glass (SG) phase, and the magnetic phase boundary correlates with the metal-insulator crossover. In complex oxides it is also well established that the $B\text{-O-B}$ bond angle governs the magnitude and sign of the magnetic exchange interaction between the neighboring B ion spins.

In the $\text{A}_2\text{Mo}_2\text{O}_7$ pyrochlores two Mo^{4+} $4d$ electrons are accommodated in the t_{2g} orbitals and play the main role for conduction and ferromagnetism. $\text{A}_2\text{Mo}_2\text{O}_7$ undergoes a magnetic transition from the SG insulating state to the FM metallic one as a function of the average ionic radius r_A , becoming FM upon increasing r_A . In this series, the compounds with lighter $A = \text{Nd, Sm, and Gd}$ show a FM behavior, with a Curie temperature T_C systematically decreasing from 90 K (Nd) to about 65 K (Gd) across the rare earth series, whereas those with $A = \text{Y}$ (or heavier) and with smaller rare earths like $A = \text{Tb, Dy, Ho, Er}$, show a SG and semiconducting behavior, with fairly high resistivity, below the

glassy transition at $T_g \sim 22, 27, 24, 21,$ and 18 K, respectively [6]. At the same time, a systematic variation of the Mo-O-Mo bond angle θ with r_A has also been observed: θ increases from 129.7° for $\text{Dy}_2\text{Mo}_2\text{O}_7$ (r_A 1.027 Å) to 131.5° for $\text{Nd}_2\text{Mo}_2\text{O}_7$ (r_A 1.109 Å), showing a stronger FM exchange interaction for larger r_A and θ values. This trend is opposite to the so-called Kanamori-Goodenough rule, which states that a larger bond angle should favor the antiferromagnetic (AFM) superexchange interaction [3,5]. Therefore, in $A_2\text{Mo}_2\text{O}_7$ the FM interaction between the Mo spins has been interpreted in terms of the double-exchange mechanism, by analogy with the same magnetic coupling observed in perovskite manganites, which selects a FM ground state upon increasing θ [3]. The dominant role of the Mo-O-Mo bond angle for the charge dynamics of the $A_2\text{Mo}_2\text{O}_7$ system was confirmed also by Raman scattering spectra [7]. Moreover, the transition of the magnetic state from FM to SG has been argued to be due to these competing double-exchange and superexchange interactions on the frustrated lattice [8,9]. It was also pointed out that both SG and FM components seem to coexist near the phase boundary of the corresponding phases [10,11], and a re-entrant transition of a SG type was observed at lower temperature and below T_C , for $A = \text{Nd}$ and Sm [11-13].

The metallic-insulating transition takes place around the $\text{Gd}_2\text{Mo}_2\text{O}_7$ composition, which is on the phase boundary between the SG and the FM regimes [14]. Due to this critical setting, this composition results to be either metallic or insulating depending on the sample preparation conditions. The FM phase can be transformed into the SG either by increasing the external pressure or by partially substituting Gd by the smaller Dy on the A site [11,15,16]. Similarly, DC resistivity measurements on single crystals show that $\text{Gd}_2\text{Mo}_2\text{O}_7$ is located on the verge of the metal-insulator transition and that it is an insulator in the ground state, differently from the other FM and metallic compositions with $A = \text{Nd}$ and Sm [16]. The FM transition is also accompanied by a magnetic irreversibility [17].

In order to determine which crystal structure parameters control the sign of the nearest-neighbor magnetic interactions and are thus responsible for the FM or SG phases in $A_2Mo_2O_7$ (with $A = \text{Gd}, \text{Dy}, \text{Ho}, \text{Er}$) and to investigate the peculiarities of the $\text{Gd}_2\text{Mo}_2\text{O}_7$ compound, we propose here a systematic and original investigation of the local structure of molybdenum-based pyrochlores by extended X-ray absorption fine structure (EXAFS) measurements. The results will, in particular, put in evidence the occurrence of an anomalous enhancement of the local structure disorder below about 225 K, thus highlighting the role played by the local structure order parameter in the stabilization of the FM and SG phases.

2. Experimental methods and data analysis

$A_2Mo_2O_7$ pyrochlore compounds were prepared by conventional solid-state reaction using different rare-earths (A), namely $A = \text{Er}^{3+}, \text{Ho}^{3+}, \text{Dy}^{3+},$ and Gd^{3+} . A_2O_3 (Metal Rare Earth Limited, 99.5%), and MoO_2 (Sigma–Aldrich, 99.9%) were used as starting raw materials. They were individually milled, in order to obtain an appropriate distribution of the particle size. Then, pyrochlore compounds with different rare-earths were weighted, and the mixture was mechanically homogenized by ball milling for 3 hours in ethanol medium in a turbula-type mixer with ZrO_2 balls with a diameter of 0.5 mm. Afterwards, the resulting powders were dried and calcined at 950 °C for 4 hours at a rate of 100 °C/min under Ar atmosphere. The calcined powders were milled again for 3 hours, and they were finally sintered in Ar atmosphere at 1350 °C for 8 hours.

A basic identification of the compound structure (cubic symmetry) was performed using X-ray diffraction (XRD, X'Pert PRO Theta/2theta of Panalytical, PANalytical, The Netherlands), see the Supplementary Material S1 for details. The patterns were recorded over the angular range 5–90° (2θ) with a step size of 0.0334° and a time per step of 100 seconds, using Cu K_α radiation ($\lambda = 0.154056$ nm) with working voltage and current of 40 kV and 100 mA, respectively. Peak positions were fitted assuming a pseudo-Voigt peak shape using the Checkcell program [18]. The lattice

parameters were refined by a global simulation of the full diagram (pattern matching, PEAKOC program) using a face-centered cubic symmetry (*fcc*) and space group $Fd\bar{3}m$ [19].

The results of the structural characterization of $A_2Mo_2O_7$ compounds are summarized in the Supplementary Material S1 as a function of the *A* ionic radii. Predictably, it should be noted that the lattice constant changes almost linearly with the radius.

The magnetic behavior of all the samples under study was checked by dc magnetometry measured by a commercial dc-squid (MPMS2 by Quantum Device). The experimental results are shown in detail in the Supplementary Material S2 and confirm the typical magnetic behavior observed in these pyrochlore compounds [3,8,13,15,20]: a SG behavior for $A = \text{Er, Ho and Dy}$ samples and a FM-like for the $A = \text{Gd}$ sample.

The EXAFS measurements were carried out at the Mo *K*-edge (20000 eV) in transmission geometry at the European Synchrotron Radiation Facility (ESRF) on beamline BM25A, using a double Si(111) crystal monochromator of the pseudo channel-cut type refrigerated at 200 K by a homemade ethanol cooling system. The energy resolution given by the monochromator was 1.2 eV. The polycrystalline $A_2Mo_2O_7$ pyrochlores were dispersed in a cellulose matrix and pressed into pellets, for optimizing the jump at the absorption edge. In order to accurately follow the behavior of the local order and structure parameters as a function of temperature, we measured accurate spectra at about 30 different temperatures in the range 8-300 K for the $Gd_2Mo_2O_7$ sample, and between 6.5 and 320 K for the Ho, Dy, and Er samples. An Oxford CV-F optistat liquid helium (LHe) cryostat with a LHe Dewar supply was used (at least three scans were collected at each temperature for averaging and checking the reproducibility). Examples of the resulting high-quality *k*-space data at several temperatures and up to 15 \AA^{-1} are shown in Fig. 1.

The EXAFS data were reduced using the Demeter package standard procedures [21]; fits of the k^2 weighted EXAFS data were carried out in *r* space using theoretical functions from the FEFF9 code [22].

To include the first and further neighbors in fitting the data (full R -fit range: 0.75 – 3.61 Å), we used the first shell Mo-O(1) peak with $R = 2.01$ Å bond length and coordination number $N_{\text{Mo-O}(1)} = 6$ (at 298 K), the Mo-Mo and Mo-A second shell peaks ($N = 6$ each), a further longer Mo-O(1) peak ($N = 6$) and one multiscattering peak. The latter was the triple forward scattering through the absorber Mo-O(1)-Mo-O(1) ($N = 6$). Alternatively, two first subshells Mo-O(1) (with coordination numbers $N_{\text{shorter}} = 2$, $N_{\text{longer}} = 4$ and lengths $R_{\text{shorter}} = 1.90$ Å, $R_{\text{longer}} = 2.00$ Å, respectively, still at 298 K) were used. This second model is in agreement with the predisposition of pyrochlores and, more in general, of complex oxides towards local disorder and B -site octahedron distortion [1,23-25]. More information on the included paths, related parameters and fit quality is provided as an example in Table 1.

Table 1. Paths, parameters, number of independent data points and R factor for the two first subshell fit of the $\text{Ho}_2\text{Mo}_2\text{O}_7$ compound at 6.5 K.

Path	N	$R(\text{Å})$	$\sigma^2(\text{Å}^2)$	N_{ind}	R-factor
Mo-O1.1	2	1.885(5)	0.00999(30)	24	0.0156
Mo-O1.1	4	2.015(5)	0.00223(7)		
Mo-Ho1.1	6	3.704(5)	0.00523(15)		
Mo-Mo1.1	6	3.698(5)	0.00488(15)		
Mo-O1.2	6	3.789(5)	0.00104(3)		
Mo-O1.1-Mo-O1.1	6	3.953(5)	0.00932(28)		

An overview of all the different paths used in our fits is shown in Fig. 2, where it is possible to appreciate their different trend as a function of the momentum transfer q . According to the EXAFS theoretical equation, the frequency of the oscillations increases with the interatomic distance R (e.g. see the difference between the Mo-O1.1-Mo and the longer Mo-Ho1.1-Mo contributions), while their amplitude increases with the coordination number and with decreasing of the local disorder σ^2 [21,22].

The initial fitting parameters were the mean-square disorder in the neighbor distances σ^2 (or “Debye-Waller parameter”), the interatomic bond lengths R , the E_0 shift in the edge energy with respect to the theoretical value and the amplitude reduction factor S_0^2 from multielectron effects. This last factor is generally between 0.8 and 1.0. At low T , the lattice is well ordered, and S_0^2 was determined from the average of several fits to scans at 8 K and fixed at 0.96. The E_0 shift was also constrained to a single value for all paths. The coordination numbers were fixed to the previously reported values for the first shell and to the crystallographic values for all the other shells and paths employed in the fit, thus reducing the uncertainty on the σ^2 parameters. This uncertainty on the local order was calculated as the statistical variance of the σ^2 parameter values obtained from the fits on the different scans collected at the same temperature, for each sample.

3. Results and discussion

In Fig. 3 the local order parameter (or shell distance variance) σ^2 for the Mo-O(1) first coordination shell obtained from the fit performed with one subshell, is reported as a function of temperature for the $\text{Gd}_2\text{Mo}_2\text{O}_7$ compound (Fig. 3, panel a) and for the three spin glasses (Fig. 3, panel b). The σ^2 behaviour of the Gd-based composition and those of the Dy, Ho and Er-based ones appear to be clearly different.

Generally speaking, the σ^2 parameter follows a temperature dependent correlated Debye-like model σ_D^2 at high temperatures, characterized by a correlated Debye temperature θ_D (that is around 800 K in these oxides), plus a temperature independent static contribution σ_S^2 due to the presence of a possibly distorted environment [24,26]. The high temperature local order parameter was fitted considering $\sigma^2(T) = \sigma_D^2 + \sigma_S^2$, as shown in Fig. 3 and already reported in previous papers [23,25,27], where the temperature dependent dynamic contribution σ_D^2 is expressed as an infinite series whose first and most important terms are [25,28]:

$$\sigma_D^2 = \frac{3\hbar^2}{Mk_B\theta_D} \left[\frac{1}{4} + \left(\frac{T}{\theta_D} \right)^2 \int_0^{\frac{\theta_D}{T}} dx \frac{x}{e^x - 1} \right] \quad (1)$$

where M is the mass of the diffuser atom and k_B is the Boltzmann constant. This model, based on σ_D^2 plus a static offset σ_S^2 , usually results to be a good approximation for all the phonon modes [28,29]. The fitting parameters were θ_D , which is a measure of the Mo-O(1) bond strength and the static offset σ_S^2 . The obtained values are reported in Table 2.

Table 2. Correlated Debye temperature θ_D and static offset σ_S^2 for the first shell Mo-O(1).

Compound	σ_S^2 (\AA^2)	θ_D (K)
Gd ₂ Mo ₂ O ₇	0.0032(3)	439(19)
Dy ₂ Mo ₂ O ₇	0.0062(3)	746(39)
Ho ₂ Mo ₂ O ₇	0.0053(3)	830(79)
Er ₂ Mo ₂ O ₇	0.0105(5)	820(50)

It is evident from Fig. 3 that the low-temperature FM Gd₂Mo₂O₇ compound exhibits a correlated Debye-like behavior only at high temperatures whereas the other three pyrochlores, which feature a higher Debye temperature (see Table 2), display a Debye-like trend at all the temperatures within the investigated range. In these last three SG compounds, the Debye temperatures are in accordance with other pyrochlore compounds [23,24,30], whereas the static contribution is quite high (see Table 2), coherently with a lattice frustration.

Therefore, the most relevant outcome is the behaviour of the σ^2 parameter, which is strictly related to the local disorder, below $T \sim 225$ K in the Gd₂Mo₂O₇ pyrochlore. From Fig. 3a, we point out that an anomalous enhancement of the local disorder with respect to the correlated Debye-like model persists down to very low temperatures. This extra σ^2 contribution amounts to 0.00358 \AA^2 at 100 K, which is about 47% of the total local disorder. Such an observation suggests that something

happens on a local scale around 225 K, determining an increase in the structural disorder. The lower value of θ_D for this composition reported in Table 2, indicates a softening of the Mo-O(1) related phonon modes that fosters the predisposition to the higher local disorder observed at low temperatures [24].

Finally, looking at Fig. 3a we further notice a peak-like trend developing around and slightly below the Curie temperature. Due to the steepness of the curve it is definitely not easy to affirm the occurrence of a magnetoelastic coupling around the FM transition but the analogies with other studied systems make us consider this possibility [23].

We have to remark that all the mentioned original features, different with respect to the local structure behavior of the SG compositions, are not simply related to the FM behaviour of $\text{Gd}_2\text{Mo}_2\text{O}_7$, as also discussed in the Supplementary Material S3 where some findings on the FM $\text{Sm}_2\text{Mo}_2\text{O}_7$ compound are shown.

Instead, the additional static contribution to the lattice disorder is similar to that observed in calcium-doped $\text{La}_{0.25}\text{Ca}_{0.75}\text{MnO}_3$ manganites below the charge ordering transition [31]. Its origin can be related to the partial symmetry breaking of the high temperature phase, with a further splitting of the Mo-O distances, which determines an additional contribution to the local order parameter.

In this context, Hodges et al. (2003) and Mirebeau et al. (2007) found in $\text{Gd}_2\text{Mo}_2\text{O}_7$, by Mössbauer spectroscopy, neutron diffraction and muon spin relaxation (μSR) measurements, an abnormal FM state with Gd^{3+} and Mo^{4+} strong spin fluctuations persisting down to low temperatures, recalling a spin-liquid-like behavior [17,32]. The continued influence of frustration is somewhat surprising since it concerns a case where the coupling between metallic ions on the *B*-sites is FM and no important single ion anisotropy is involved. It is possible that the frustration is linked either to the role of further AFM neighbouring interactions or to the proximity of a quantum phase transition [32]. Frustration is thus still operating in this essentially isotropic pyrochlore where the dominant Mo intra-sublattice interaction is FM. Therefore, the present results confirm that $\text{Gd}_2\text{Mo}_2\text{O}_7$ is a

peculiar composition where the competition between order and disorder, typical of pyrochlores, gives rise to unique features in the local structure [23].

Moreover, in the literature the studies performed on all these $A_2\text{Mo}_2\text{O}_7$ systems by other spectroscopic techniques at temperatures above 150-200 K are very rare. The reason of this lack is due to the absence, in this higher T range, of any peculiar feature in the resistivity and magnetization, whereas the research is much more extensive at lower temperatures where all the SG and magnetic transitions occur. Our findings add a further focus on this less explored higher temperature region.

In order to gain a deeper insight of the structural disorder of the explored compounds, we hypothesize the presence of at least a bimodal distribution of the Mo-O(1) interatomic distances for the first shell $\text{MoO}(1)_6$ octahedra according to the two subshell fit model described in the experimental section and similar to what we used for Ru-pyrochlores [23,33].

In fact, whereas X-ray powder diffraction experiments, giving medium- to long-range information, show the presence of six identical Mo-O(1) interatomic distances [3], Higashiya et al. (2007) emphasized how in $A_2\text{Mo}_2\text{O}_7$ with $A = \text{Nd, Sm, Gd, Tb, and Y}$, the $\text{MoO}(1)_6$ octahedron should be further trigonally distorted or squeezed in such a way that one pair of opposite faces are pushed together [6,34].

Actually, our EXAFS results show two shorter apical and four longer basal first shell Mo-O(1) interatomic distances (Fig. 4) and, in the second coordination shell, six longer Mo-Mo and six shorter Mo-A bond lengths (see Supplementary Material S4 for more details). This behavior indicates that an octahedral distortion is present for all the studied compositions. We point out that the difference between the two Mo-O(1) subshells is of about 0.150 \AA , i.e. well above the widely recognized ΔR limit determined by the EXAFS resolving power between two scattering shells involving the same chemical species at different distances, $\Delta R \geq \pi/2k_{\text{max}}$, where k_{max} is the maximum k vector used. Since for our data $k_{\text{max}} = 15 \text{ \AA}^{-1}$, we are able to accurately resolve splittings down to 0.105 \AA [35,36].

In Fig. 4 we also observe that the two shorter apical interatomic Mo-O(1) distances slightly decrease at high temperature in $\text{Gd}_2\text{Mo}_2\text{O}_7$ whereas they slightly increase in $\text{Dy}_2\text{Mo}_2\text{O}_7$. This could be, apart from an experimental scattering of data points, a further fingerprint of what happens in the local disorder σ^2 behaviour and then in the distribution of distances around 225 K, as shown in Fig. 3. We hypothesize that at high temperature the symmetry breaking of the $\text{MoO}(1)_6$ octahedron, described by the bimodal distribution of 2+4 interatomic distances, is sensitive to the decreasing ionic radius going from the low-temperature FM regime of $\text{Gd}_2\text{Mo}_2\text{O}_7$ to the SG one which starts in the lanthanides period with $\text{Dy}_2\text{Mo}_2\text{O}_7$.

Finally, the local order parameters $\sigma^2(T)$ of the second shell peaks Mo-Mo and Mo-A have a monotonic behaviour and do not show any anomaly in the one subshell fit, as already observed in other pyrochlores compositions [23].

4. Conclusions

In summary, we have performed temperature dependent EXAFS measurements at the Mo *K*-edge on four Mo-based pyrochlores providing relevant information on the local order and structure for the first and second neighbor shells. The measurements show an anomalous lattice disorder below $T \sim 225$ K in the first shell of the low-temperature FM $\text{Gd}_2\text{Mo}_2\text{O}_7$ system probably related to the criticality of this peculiar composition located on the border between the SG and the FM regimes. In particular, we might be observing a remnant fingerprint, on a local scale, of the SG or frustrated phase that is typically seen for ionic radii just below that of Gd. In the other three SG compounds ($\text{Dy}_2\text{Mo}_2\text{O}_7$, $\text{Ho}_2\text{Mo}_2\text{O}_7$ and $\text{Er}_2\text{Mo}_2\text{O}_7$), the Debye temperatures are in agreement with other pyrochlores whereas the static local order contribution is compatible with a lattice frustration. Moreover, an octahedral distortion is observed for all the studied compositions, pointing out two shorter and four longer first shell Mo-O(1) interatomic distances. All these findings are coherent with the tendency of pyrochlores to develop a structural distortion [23,37].

Therefore, our results foster the conclusion that the sign of the nearest-neighbor magnetic interactions and the FM or SG phases stabilization are strictly related on a local scale to the structure order parameter.

Acknowledgments

We gratefully acknowledge the Spanish CRG at the ESRF for providing beamtime under experiment HC-2414. F.R.-M. is also indebted to MINECO for a ‘Ramon y Cajal’ contract (ref: RyC-2015-18626), which is co-financed by the European Social Fund. G.L. thanks M. Lucaccini and G. Tavilla for their valuable technical support and C. Robustelli for the supply of cryogenic liquids during the magnetization measurements.

References

- [1] J. S. Gardner, M. J. P. Gingras, J. E. Greedan, *Rev. Mod. Phys.* 82 (2010) 53.
- [2] Mark T. Weller, R. W. Hughes, J. Rooke, C. S. Knee and Jon Reading, *Dalton Trans.* (2004) 3032.
- [3] Y. Moritomo, Sh. Xu, A. Machida, T. Katsufuji, E. Nishibori, M. Takata, M. Sakata, S-W. Cheong, *Phys. Rev. B* 63 (2001) 144425.
- [4] Y. Shimakawa and Y. Kubo, N. Hamada, J. D. Jorgensen, Z. Hu, and S. Short, M. Nohara and H. Takagi, *Phys. Rev. B* 59 (1999) 1249.
- [5] J. B. Goodenough, *J. Phys. Chem. Solids* 6 (1958) 287.
- [6] A. Higashiya, S. Imada, A. Yamasaki, A. Irizawa, A. Sekiyama, S. Suga, Y. Taguchi, M. Iwama, K. Ohgushi, Y. Tokura, *Phys. Rev. B* 75 (2007) 155106.
- [7] K. Taniguchi, T. Katsufuji, S. Iguchi, Y. Taguchi, H. Takagi, and Y. Tokura, *Phys. Rev. B* 70 (2004) 100401(R).
- [8] S. Iguchi, N. Hanasaki, M. Kinuhara, N. Takeshita, C. Terakura, Y. Taguchi, H. Takagi, and Y. Tokura, *Phys. Rev. Lett.* 102 (2009) 136407.
- [9] Yukitoshi Motome and Nobuo Furukawa, *Phys. Rev. Lett.* 104 (2010) 106407.
- [10] T. Katsufuji, H.Y. Hwang, and S-W. Cheong, *Phys. Rev. Lett.* 84 (2000) 1998.
- [11] J.-G. Park, Younghun Jo, Junghwan Park, H.C. Kim, H.-C. Ri, Sh. Xu, Y. Moritomo, S.-W. Cheong, *Physica B* 328 (2003) 90.
- [12] N. Hanasaki, K. Watanabe, T. Ohtsuka, I. Kézsmárki, S. Iguchi, S. Miyasaka, and Y. Tokura, *Phys. Rev. Lett.* 99 (2007) 086401.
- [13] G. Prando, P. Carretta, A. U. B. Wolter, R. Saint-Martin, A. Revcolevschi, and B. Büchner, *Phys. Rev. B* 90 (2014) 085111.
- [14] N. Hanasaki, M. Kinuhara, I. Kézsmárki, S. Iguchi, S. Miyasaka, N. Takeshita, *Phys. Rev. Lett.* 96 (2006) 116403.
- [15] I. Mirebeau, A. Apetrei, I. Goncharenko, D. Andreica, P. Bonville, J. P. Sanchez, A. Amato, E. Suard, W. A. Crichton, A. Forget, and D. Colson, *Phys. Rev. B* 74 (2006) 174414.
- [16] I. Kézsmárki, N. Hanasaki, D. Hashimoto, S. Iguchi, Y. Taguchi, S. Miyasaka, and Y. Tokura, *Phys. Rev. Lett.* 93 (2004) 266401.
- [17] J.A. Hodges, P. Bonville, A. Forget, J.P. Sanchez, P. Vulliet, M. Rams, and K. Królas, *Eur. Phys. J. B* 33 (2003) 173.
- [18] Single Crystal and Powder Diffraction – Freely Available Crystallographic Software for Academia: <http://www.ccp14.ac.uk/mirror/mirror.htm>
- [19] O. Masson, Peakoc profile fitting program, 2008, <http://www.esrf.eu/UsersAndScience/Experiments/TBS/SciSoft/OurSoftware/PEAKOC>
- [20] N. Ali, M.P Hill, S. Labroo, J.E Greedan, *Journal of Solid State Chemistry* 83 (1989) 178.
- [21] B. Ravel and M. Newville, *J. Synchrotron Radiat.* 12 (2005) 537.
- [22] J.J. Rehr, J.J. Kas, F.D. Vila, M.P. Prange, K. Jorissen, *Phys. Chem. Chem. Phys.* 12 (2010) 5503.
- [23] C. Castellano, G. Berti, S. Sanna, R. Ruiz-Bustos, J. van Duijn, A. Brambilla, Á. Muñoz-Noval, P. Carretta, L. Duò, and F. Demartin, *Phys. Rev. B* 91 (2015) 224101.
- [24] C. H. Booth, J. S. Gardner, G. H. Kwei, R. H. Heffner, F. Bridges, and M. A. Subramanian, *Phys. Rev. B* 62 (2000) R755.
- [25] C. Castellano, M. Ferretti, A. Martinelli, and M. R. Cimberle, *J. Alloys Compd.* 478 (2009) 479.
- [26] E. D. Crozier, J. J. Rehr, and R. Ingalls, in: D. Koningsberger and R. Prins (Eds.), *X-Ray Absorption: Principles, Applications, Techniques of EXAFS, SEXAFS, XANES*, Wiley, New York, 1988, pp. 373-442.
- [27] C. Castellano, G. Berti, M. Ferretti, A. Martinelli, M. R. Cimberle, *J. Alloys Compd.* 663 (2016) 560.

- [28] G. Beni and P. M. Platzmann, *Phys. Rev. B* 14 (1976) 1514.
- [29] N. W. Ashcroft and N. D. Mermin, in *Solid State Physics* (Saunders College, Philadelphia, 1976).
- [30] M. B. Johnson, D. D. James, A. Bourque, H. A. Dabkowska, B. D. Gaulin, and M. A. White, *J. Solid State Chem.* 182 (2009) 725.
- [31] C. Castellano, A. Paolone, F. Cordero, R. Cantelli, M. Ferretti, *Solid State Commun.* 129 (2004) 143.
- [32] I. Mirebeau, A. Apetrei, I. Goncharenko, D. Andreica, P. Bonville, *J. Magn. Magn. Mater.* 310 (2007) 919.
- [33] G. Berti, S. Sanna, R. Ruiz-Bustos, J. van Duijn, A. Brambilla, Á. Muñoz-Noval, F. Demartin, L. Duò and C. Castellano, *RSC Adv.* 5 (2015) 100809.
- [34] I. V. Solovyev, *Phys. Rev. B* 67 (2003) 174406.
- [35] P. A. Lee, P. H. Citrin, P. Eisenberger, and B. M. Kincaid, *Rev. Mod. Phys.* 53 (1981) 769.
- [36] T. Keiber, F. Bridges, and B. C. Sales, *Phys. Rev. Lett.* 111 (2013) 095504.
- [37] P. E. R. Blanchard, R. Clements, B. J. Kennedy, C. D. Ling, E. Reynolds, M. Avdeev, A. P. J. Stampfl, Z. Zhang, and L.-Y. Jang, *Inorg. Chem.* 51 (2012) 13237.

Figure Captions

Fig. 1. (Color online) $k^2\chi(k)$ EXAFS signals at all the measured temperatures between 8 K (lower curve) and 298 K (upper curve), for the $\text{Ho}_2\text{Mo}_2\text{O}_7$ compound. Data were offset for clarity.

Fig. 2. (Color online) Back Fourier transform best-fit curve and single fit contributions for the spectrum taken at 6.5 K on $\text{Ho}_2\text{Mo}_2\text{O}_7$. Letters refer to different paths as follows: (a) Data + fit; (b) Mo–O1.1–Mo (2 atoms); (c) Mo–Ho1.1–Mo; (d) Mo–Mo1.1–Mo; (e) Mo–O1.2–Mo; (f) Mo–O1.1–Mo–O1.1–Mo; (g) Mo–O1.1–Mo (4 atoms). Data have been offset for clarity.

Fig. 3. (Color online) Mo–O(1) first shell σ^2 (\AA^2) as a function of temperature for a) $\text{Gd}_2\text{Mo}_2\text{O}_7$ and b) the three spin-glass compositions. The continuous line is the fit at high temperatures to a correlated Debye model plus a static offset. The axis scale is the same in both panels.

Fig. 4. (Color online) Bimodal distribution of the first shell Mo–O(1) interatomic distances [$N_{\text{Mo–O}} = 2$ shorter apical (solid circles) and $N_{\text{Mo–O}} = 4$ longer basal (open circles) interatomic distances]. The dashed lines are the crystallographic values of the interatomic distances and the statistical errors are equal to the dimensions of the circles.

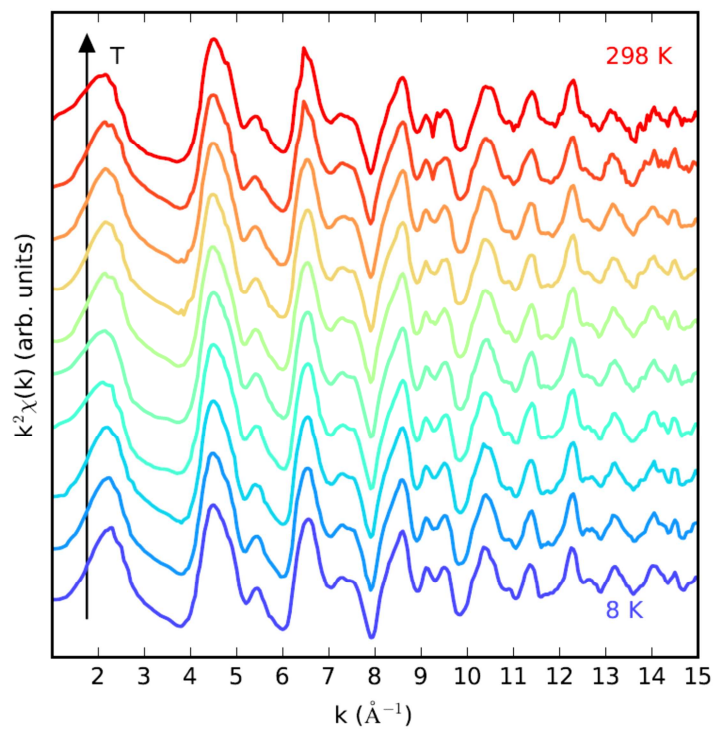


Fig. 1.

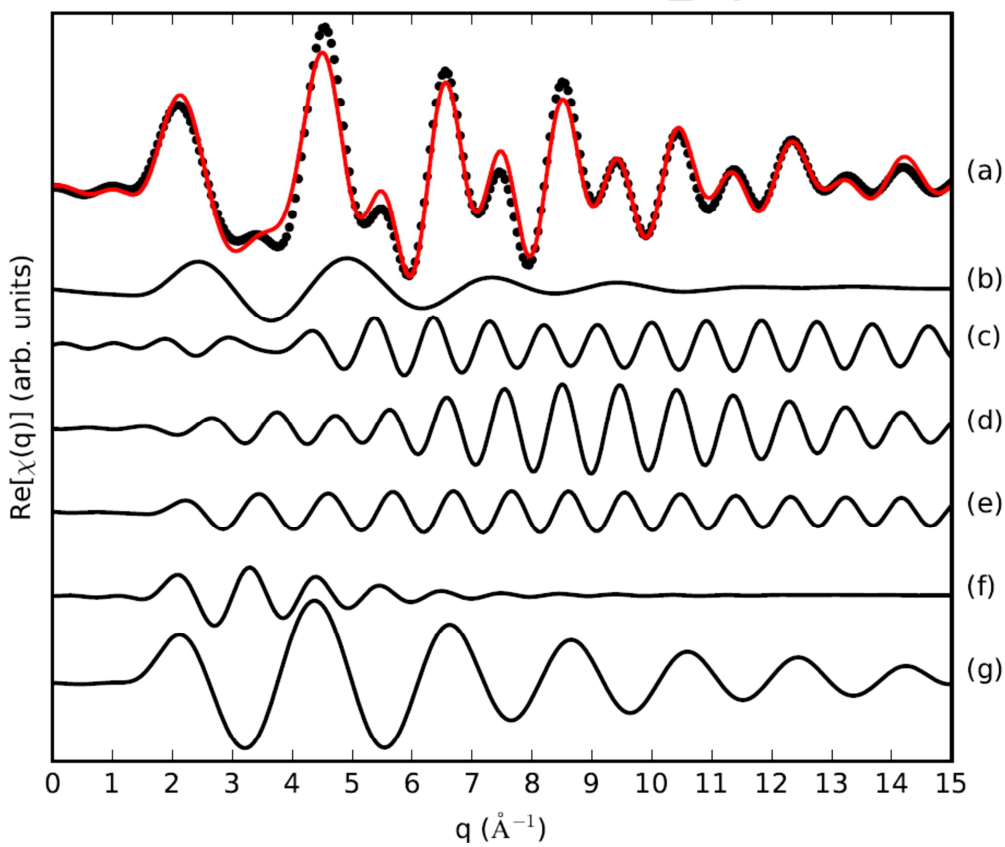


Fig. 2.

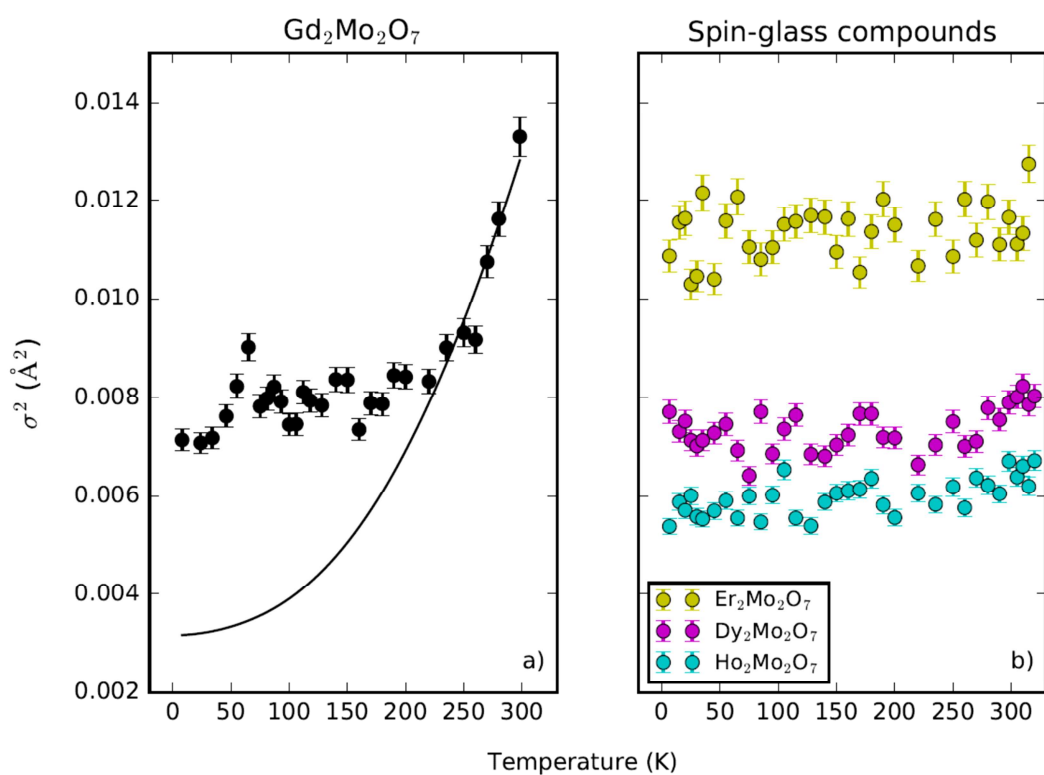


Fig. 3.

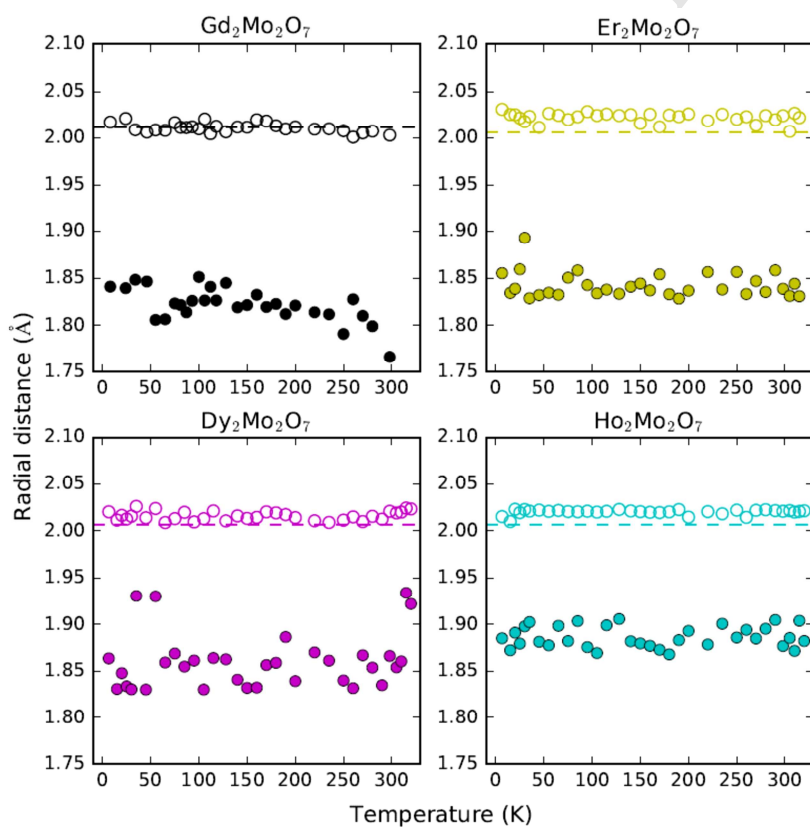


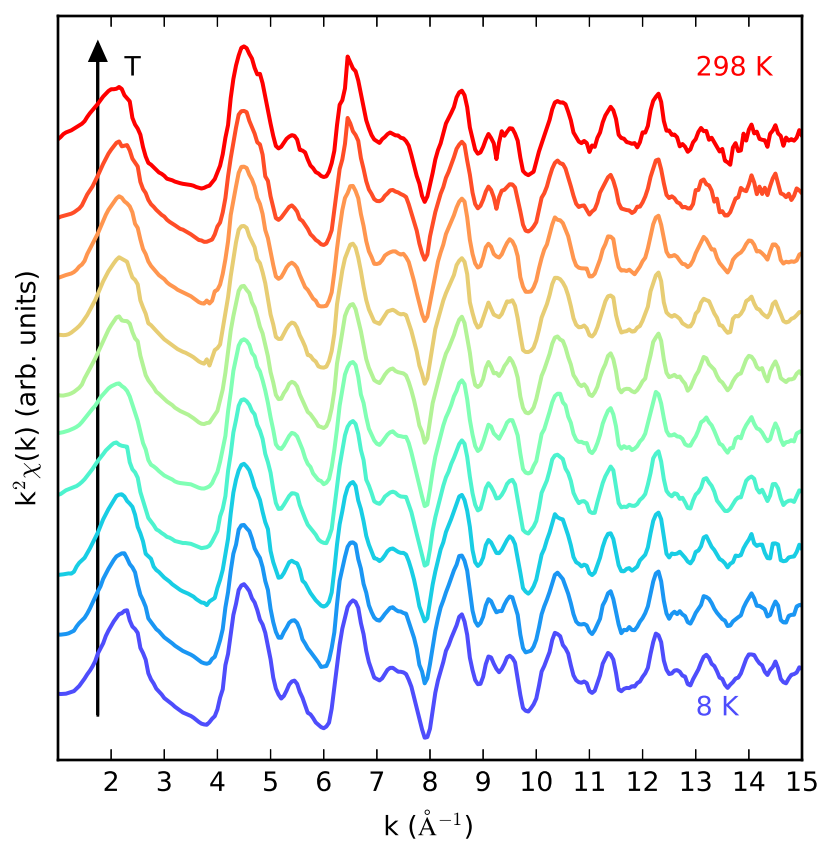
Fig. 4.

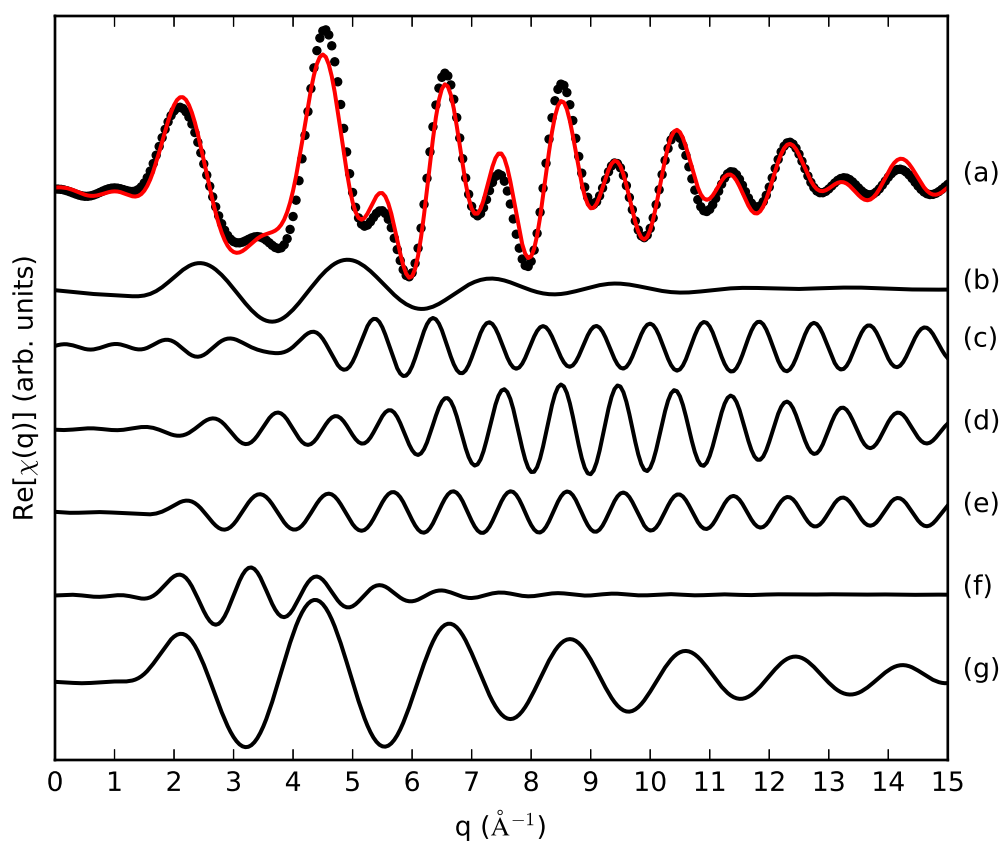
Table 1. Paths, parameters, number of independent data points and R factor for the two first subshell fit of the $\text{Ho}_2\text{Mo}_2\text{O}_7$ compound at 6.5 K.

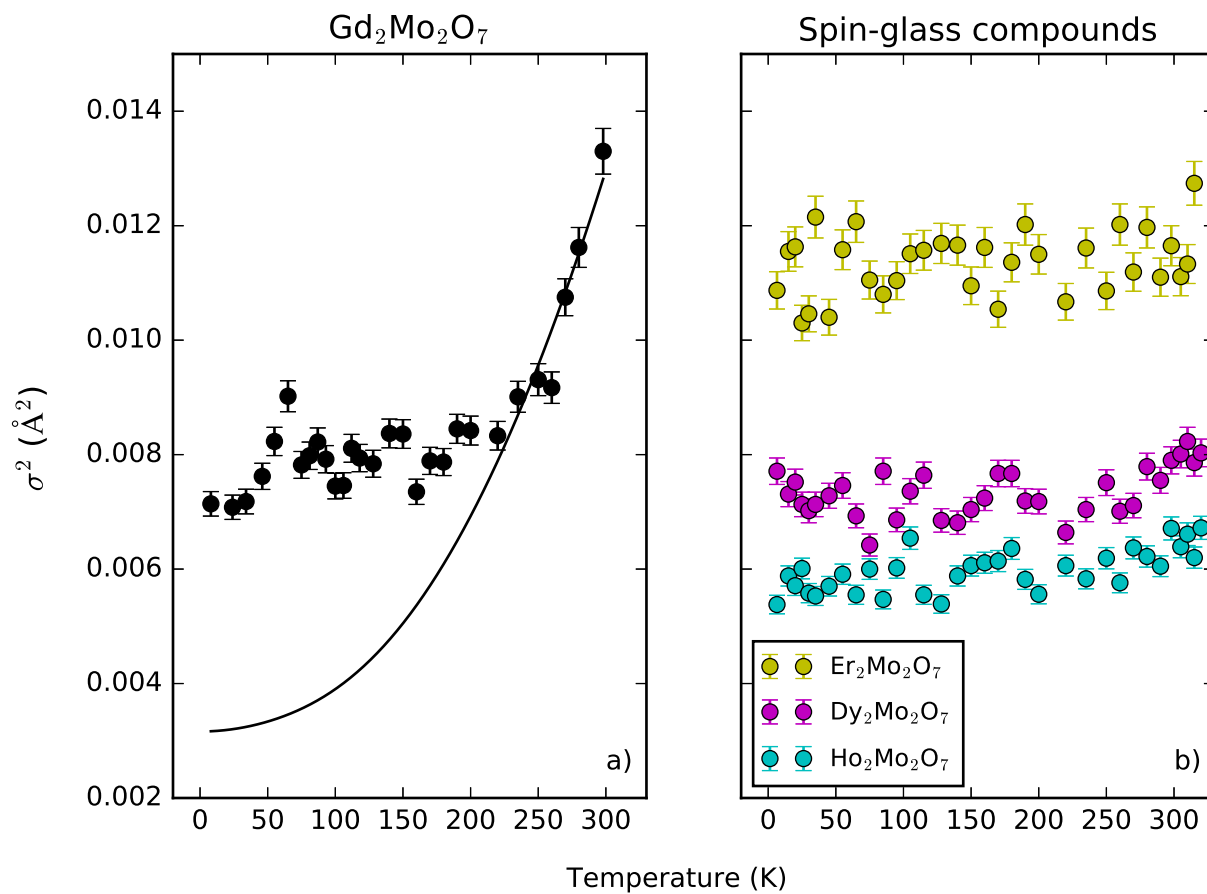
Path	N	R(\AA)	$\sigma^2(\text{\AA}^2)$	N_{ind}	R-factor
Mo-O1.1	2	1.885(5)	0.00999(30)	24	0.0156
Mo-O1.1	4	2.015(5)	0.00223(7)		
Mo-Ho1.1	6	3.704(5)	0.00523(15)		
Mo-Mo1.1	6	3.698(5)	0.00488(15)		
Mo-O1.2	6	3.789(5)	0.00104(3)		
Mo-O1.1-Mo-O1.1	6	3.953(5)	0.00932(28)		

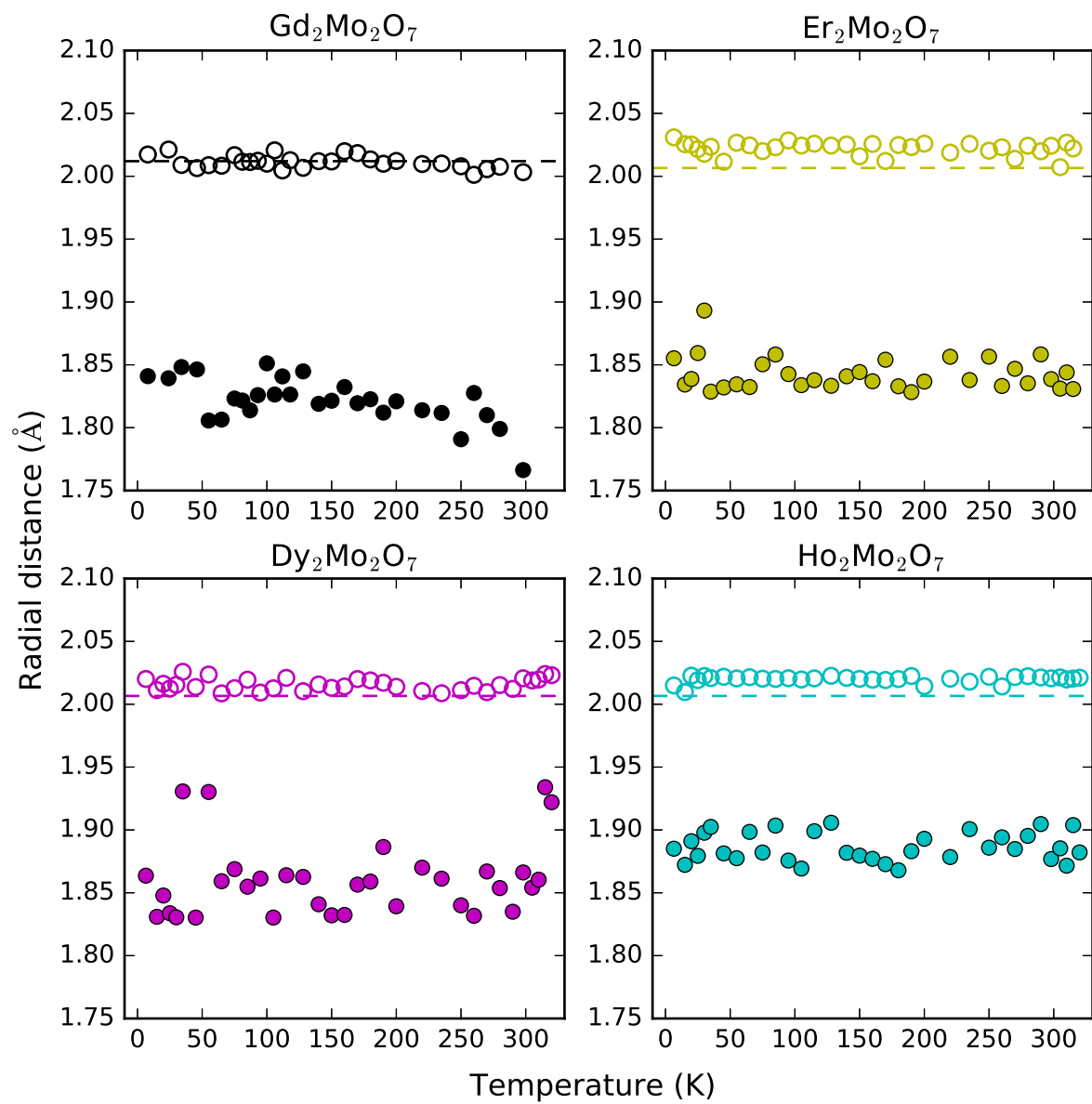
Table 2. Correlated Debye temperature θ_D and static offset σ_S^2 for the first shell Mo-O(1).

Compound	σ_S^2 (\AA^2)	θ_D (K)
Gd ₂ Mo ₂ O ₇	0.0032(3)	439(19)
Dy ₂ Mo ₂ O ₇	0.0062(3)	746(39)
Ho ₂ Mo ₂ O ₇	0.0053(3)	830(79)
Er ₂ Mo ₂ O ₇	0.0105(5)	820(50)









Ferromagnetic $\text{Gd}_2\text{Mo}_2\text{O}_7$ shows an enhancement of the local disorder below 225 K.

A MoO_6 octahedral distortion is observed for all the studied compounds.

The general pyrochlore predisposition towards structural disorder is verified.